

Research Repository

Rational discovery of a SOD1 tryptophan oxidation inhibitor with therapeutic potential for amyotrophic lateral sclerosis

Accepted for publication in the Journal of Biomolecular Structure and Dynamics.

Research Repository link: <https://repository.essex.ac.uk/34767/>

Please note:

Changes made as a result of publishing processes such as copy-editing, formatting and page numbers may not be reflected in this version. For the definitive version of this publication, please refer to the published source. You are advised to consult the published version if you wish to cite this paper.

<https://doi.org/10.1080/07391102.2018.1531787>

1 **Rational discovery of a SOD1 tryptophan oxidation inhibitor with**
2 **therapeutic potential for amyotrophic lateral sclerosis**
3

4 **Ramu Manjula^{1#}, Sruthi Unni^{1#}, Gareth S. A. Wright², M. M. Srinivas Bharath^{3,4}**
5 **and Balasundaram Padmanabhan^{1*}**

6
7 ¹Department of Biophysics, ³Department of Neurochemistry, National Institute of Mental
8 Health and Neurosciences (NIMHANS), Hosur Road, Bangalore – 560029, India.

9 ²Molecular Biophysics Group, Institute of Integrative Biology, Faculty of Health and Life
10 Sciences, University of Liverpool, Liverpool L69 7ZB, UK.

11 ³Neurotoxicology Laboratory, Neurobiology Research Center, National Institute of Mental
12 Health and Neurosciences (NIMHANS), Hosur Road, Bangalore – 560029, India.

13
14
15 **#Equally contributed**

16 ***To whom correspondence should be addressed**

17
18 Tel: +91-80-26995102, Fax: +91-80-26564830

19
20 **E-mail: paddy@nimhans.ac.in or balapaddy@gmail.com**

1 **ABSTRACT**

2 Formation of Cu, Zn superoxide dismutase 1 (SOD1) protein inclusions within motor neurons
3 is one of the principal characteristics of SOD1-related amyotrophic lateral sclerosis (ALS). A
4 hypothesis as to the nature of SOD1 aggregation implicates oxidative damage to a solvent-
5 exposed tryptophan as causative. Here, we chart discovery of a phenanthridinone based
6 compound (Lig9) from the NCI Diversity Set III by rational methods by *in silico* screening and
7 crystallographic validation. The crystal structure of the complex with SOD1, refined to 2.5 Å,
8 revealed that Lig9 binds the SOD1 β -barrel in the β -strand 2 and 3 region which is known to
9 scaffold SOD1 fibrillation. The phenanthridinone moiety makes a substantial $\pi - \pi$ interaction
10 with Trp32 of SOD1. The compound possesses significant binding affinity for SOD1 and
11 inhibits oxidation of Trp32; a critical residue for SOD1 aggregation. Thus, Lig9 is a good
12 candidate from which to develop a new library of SOD1 aggregation inhibitors through
13 protection of Trp32 oxidation.

14

15 **Keywords:** ALS, SOD1; Trp oxidation; Modulators; NCI diversity set, Virtual screening,
16 Phenanthridinone derivative, Crystal structure; Binding assay

17

1 **1. Introduction**

2 Amyotrophic lateral sclerosis (ALS) is a neurodegenerative disorder involving motor neuron
3 degeneration that leads to progressive muscle weakness and paralysis. Ultimately, respiratory
4 failure leads to death (Brown and Al-Chalabi, 2017). The timing of disease onset is variable;
5 however, patients usually die within 3-5 years of symptom onset. A familial form of ALS can
6 caused by mutations in the superoxide dismutase-1 (SOD1) protein. Mutant SOD1 protein
7 induces the formation of abundant neuronal cytoplasmic protein aggregates in human patients
8 and transgenic mouse model (Bruijn et al., 1998; Kato et al., 1996). Proteomic analysis of
9 aggregates from spinal cord sections in ALS mouse models shows they contain mutant SOD1
10 proteins in addition to unmodified, full length, wild-type SOD1 polypeptides (Shaw et al.,
11 2008). Over 150 different disease mutations have been reported in the *SOD1* gene. Some of
12 these mutations have been shown to negatively affect native SOD1 homodimer stability.
13 Structural instability of SOD1 potentially results in homologous (Lang et al., 2015; Deng et al.,
14 1993; Banci et al., 2008; Kim et al., 2015) or heterologous (Fujisawa et al., 2012; Nishitoh et
15 al., 2008) protein aggregation. Mutations are also associated with a decreased metal binding
16 (Lindberg et al., 2002; Johnston et al., 2000) and misplaced disulfide formation (Tiwari and
17 Hayward 2003; Niwa et al., 2007; Cozzolino et al., 2008). Metal loss increases the
18 conformational flexibility of both electrostatic and zinc-binding loops exposing the β -barrel
19 core, possibly causing non-native interactions leading to aggregation (Strange et al., 2007).

20 SOD1 bears only one tryptophan (Trp32) which is found in β -strand 2 exposed to
21 solvent on the surface of the protein. This region is pathophysiologically important as it forms
22 repeating anti-parallel β -sheet structures and is found at the core of SOD1 aggregates (Sangwan
23 et al., 2017). Mutational studies have revealed that Trp32 oxidation is a crucial factor in the
24 bicarbonate-dependent, covalent aggregation of SOD1 (Zhang et al., 2003). Intriguingly,
25 oxidative post-translational modification of Trp32 to kynurenine and N-formyl kynurenine

1 results in the covalent crosslinking of oxidized SOD1 monomers (Zhang et al., 2003). The
2 proclivity of SOD1 Trp32 to undergo oxidation has gained significance due to its detection in
3 ALS mouse models with mutant SOD1 (Johnston et al., 2000). Compared to any other position
4 32 variants, oxidation profoundly increases SOD1 aggregation (Taylor et al., 2007; Grad et al.,
5 2011) indicating that inhibition of Trp oxidation could be a potential therapeutic target to
6 prevent aggregation and slow disease progression in ALS.

7 Considerable effort has been expended to discover a successful drug against ALS. The
8 only two FDA approved drugs to slow down the disease progression in ALS are Rilutek
9 (riluzole) and Radicava (edaravone) (Traynor, 2017). However, the effect of riluzole is modest
10 with only 9% gain in survival for a year after the initiation of treatment (Messori et al., 1999).
11 There is, therefore, an urgent need for new SOD1 modulators for the treatment of ALS.
12 Clioquinol and PBT2 are two of the many kynurenine pathway inhibitors designed as to treat
13 ALS based on their structural similarity with kynurenine and quinolinic acid respectively (Chen
14 & Guillemin, 2012). The latter products are catabolites involved in tryptophan oxidation to
15 form N-formyl kynurenine. Tryptophan oxidation protection conferred by various natural
16 antioxidant phenolics has also been studied (Salminen & Heinonen, 2008) but not implemented
17 as a therapy. In addition, a Trp32 targeted drug molecule, 5-fluorouridine, has been shown to
18 reduce SOD1 aggregation in human cell culture (Pokrishevsky et al., 2017) despite low binding
19 affinities (Wright et al., 2013). This study addressed the demand for quantifiable protein-ligand
20 interactions targeted to the Trp32 site with therapeutic applications in ALS. However, small
21 molecules with optimal inhibitory effect on SOD1 and Trp32 oxidation and the structural basis
22 of such inhibitors have not been extensively studied.

23 To address this and find structurally diverse molecules targeted to SOD1, we carried
24 out structure-based virtual screening of the NCI Diversity Set III library followed by X-ray

- 1 crystallographic validation to obtain novel SOD1 modulators. This search identified a small
- 2 molecule phenanthridinone derivative SOD1 modulator (NSC127133; hereafter, Lig9).

1 **Materials and methods**

2 *Virtual screening of NCI database*

3 The crystal structure of a previously determined SOD1-inhibitor complex (PDB Id: 5YTO)
4 was used for docking studies (reference). Protein preparation for computational studies
5 included removal of the ligand from the binding site, addition of protein hydrogens, bond
6 optimization and energy minimization. The grid box for the docking process was created using
7 the Autodock/Vina plugin for PyMol (Seeliger & de Groot, 2010). The docking grid-box was
8 centered at the Trp32 residue with a box size of 22.50 x 22.50 x 22.50 Å that covers the entire
9 binding site around Trp32. The database of 1620 compounds of the NCI diversity set III were
10 retrieved and prepared using AutoDock utilities. The screened molecules, subjected to the
11 Lipinski Rule of Five, were docked against the receptor site using AutoDock Vina (Trott &
12 Olson, 2010). The resultant poses were analyzed based on cut off docking score values and
13 subsequent visual inspection for an accurate understanding of intermolecular interactions
14 between SOD1 and ligands. The shortlisted ligands from the *in-silico* analysis were procured
15 from the National Cancer Research Institute at Bethesda, USA.

16 *Biological section*

17 *Reagents*

18 A SOD1 expression plasmid encoding a tobacco etch virus (TEV) protease cleavable His tag-
19 SOD1 fusion protein was generated by ligation of the SOD1 DNA coding sequence in frame
20 between the NcoI and XhoI sites in the pETM-11 vector. All the chemicals, unless specified,
21 were purchased from Sigma, India.

22 *Gene expression and protein purification*

23 SOD1 was expressed in *E. coli* strain BL21 star (DE3) (Stratagene). *E. coli* cells were grown
24 at 37 °C until its optical density at 600 nm reached 0.6 and then SOD1 expression was induced
25 by addition of 0.4 mM IPTG (isopropyl β-D-1-thiogalactopyranoside) at 20 °C overnight. Cells

1 were harvested by centrifugation and the pellet was stored at -80° C. Cells were lysed in 20mM
2 Tris HCl, 300mM NaCl, 5mM β -mercaptoethanol, pH 7.5 by sonication (Vibra cell) at 30 %
3 amplitude with 3 second pulse and 5 second rest. The supernatant was loaded onto a Ni-NTA
4 column (HisTrap FF, GE Healthcare, USA) for metal affinity purification and eluted with 200
5 mM of Imidazole. TEV protease was used to remove the His-tag by incubation with the former
6 at 4 °C on a rocker overnight then concentrated and separated from remaining impurities by
7 size exclusion chromatography (Superdex 75G 16/60 from GE Healthcare, USA) on an AKTA
8 Prime Plus (GE Healthcare, USA).

9 ***Ligand soaking and X-ray crystallography***

10 The SOD1 protein, with a concentration of 8-9 mg/ml in 20 mM Tris pH 8.0, was crystallized
11 by the hanging-drop method. Drops consisting of 2 μ l protein mixed with 2 μ l reservoir solution
12 in 24-well plates were equilibrated against a 500 μ l reservoir solution of sodium citrate pH 6.0.

13 Crystals were then soaked separately with the five compounds (50 mM stock) dissolved
14 in 1.5 M sodium citrate pH 6.0 for 3 hours, 6 hours and overnight at 20 °C. X-ray
15 crystallographic data sets were collected on a RAXIS IV++ diffractometer (Rigaku
16 Corporation, Japan) at NCBS, Bangalore. Diffraction data were integrated and scaled using
17 HKL2000 (Minor and Otwinowski, 1997). The crystals belong to the space group $C222_1$, with
18 cell dimensions of $a = 164.36 \text{ \AA}$, $b = 203.69 \text{ \AA}$ and $c = 144.21 \text{ \AA}$. The crystal structures were
19 solved by molecular replacement using Molrep (Vagin & Teplyakov, 1997) in the CCP4
20 software package (Collaborative Computational Project, Number 4, 1994). The intact dimer
21 structure of SOD1 (PDB Id: 5YTO) (Manjula et al., 2018) was used as the search model. The
22 structure solution yielded five SOD1 dimers in the asymmetric unit, for all the five crystals
23 tested. The $2|F_o| - |F_c|$ and the difference Fourier $|F_o| - |F_c|$ maps were carefully analyzed. No
24 electron density was found corresponding to any of the compounds except for compound, Lig9.

1 Energy minimized coordinates and crystal information files (CIF) for Lig9 were produced
2 using Jligand (Lebedev et al., 2012).

3 The structure of the SOD1 complex was refined using the *Phenix.refine* (Terwilliger et
4 al., 2008) then *REFMAC5* (Murshudov et al., 1997). A few rounds of refinement cycles and
5 model building using Coot (Emsley et al., 2004) were performed to obtain the final structure.
6 The final refined structure of the SOD1 complex in the asymmetric unit contains 11081 protein
7 atoms, nine Zn²⁺ ions, four glycerol molecules, three polysulfane molecules and 1324 water
8 molecules, with a final R_{work} of 16.6 % and an R_{free} of 23.7 % at 2.5 Å resolution. The
9 stereochemistry of these crystal structures is good, as assessed with *MOLPROBITY* (Chen et
10 al., 2010). The X-ray data collection, scaling and refinement statistics are summarized in Table
11 2. The structural coordinates of the SOD1 – Lig9 complex has been deposited in the RCSB
12 (PDB Id: 6A9O).

13 14 ***Molecular dynamic (MD) simulations***

15 The crystal structure of the SOD1-Lig9 complex, determined in the present study, was used to
16 perform MD simulations to check ligand interaction stability at the binding site in the presence
17 or absence of SOD1-Trp32. The Desmond program from the D. E. Shaw group was used to
18 perform the MD simulation. A tryptophan-32 to alanine mutant SOD1 protein structure was
19 generated in Maestro. The wild-type and W32A SOD1 structures were minimized and checked
20 for other penalties including the addition of hydrogens. The simulation box set up was cuboidal
21 in nature with the minimum number of solvent molecules added to the protein. The solvated
22 water box was generated and minimized using the steepest descent method until a gradient
23 threshold of 1.0 kcal/mol/Å was reached with a minimum step size of 10. The Coulombic
24 interactions were cutoff at 9.0 Å. Default force constant was applied and no other restraints on
25 the protein and solvent molecules were applied during the minimization process. The
26 production run consisted of 8 stages including relaxation of the complete system before the

1 simulation run and was performed at 300 K and 1.01325 bar pressure. The production run was
2 carried out for a period of 50ns. The trajectory was saved at a step size of 4.8 ps/frame which
3 generated about 10,417 frames. The trajectory was analyzed using both the Desmond and
4 Maestro programs from the Schrodinger software package (Desmond, 2015).

5
6 ***Surface plasmon resonance (SPR) assay***

7 SPR assay was performed to check the binding efficiency of the selected 20 compounds
8 (Supplementary Table 1) against SOD1 using a Biacore T200 or Biacore 3000 (GE Healthcare,
9 USA) instruments. The immobilization was performed using purified SOD1. Reference
10 surfaces were prepared by blocking carboxyls on the sensor chip, and no protein was added.
11 Ligand molecule (analyte) was allowed to flow over the immobilized-protein surface, and the
12 binding response of analyte to protein was recorded. The chip surface was regenerated by the
13 removal of the analyte with regeneration buffer. Initially, a single concentration was used to
14 check binding response and different compounds were taken in 100 µg/ml concentration. The
15 maximum response with each analyte reflects relative binding affinity. To analyze the dose
16 dependency of the Lig9 compound, different concentrations were used. The final response of
17 bound protein, expressed in response units (RU), was calculated by subtraction of the reference
18 RU. PBS with 5% DMSO was used as both running and analyte binding buffer. 250 µM and
19 125 µM concentrations of Lig9 were used to compare the binding efficiency between wild-
20 type SOD1 and W32A mutant.

21
22 ***Microscale thermophoresis (MST) assay***

23 SOD1 was labeled with a fluorescent dye, NT-647. The dye NT-647 labels the primary amine
24 groups on lysine residues of the protein. The dye was dissolved in DMSO and diluted with 1X
25 MST buffer with 0.05 % Tween-20. 100 µl of 20 µM protein was then mixed with 100 µl of
26 diluted dye, and the reaction mixtures were incubated for 30 min at room temperature in the

1 dark. Unreacted dye was removed using PD10 desalting columns, and the capillary scan was
2 performed for labeled protein to check its fluorescence.

3 A stock solution of Lig9 with a concentration of 20 mM was prepared in 100 % DMSO.
4 5 mM of Lig9 was prepared in TBS buffer in 10 μ l volume, and it was serially diluted (two-
5 fold each time) 16 fold in TBS containing 10% DMSO, followed by adding an equal amount
6 of labeled SOD1 (100 nM) to each titration. The mixed samples were loaded into Monolith
7 NT.115 capillaries, and subjected to MST analysis using a Monolith NT.115 (NanoTemper
8 Technologies), performed at MST power of 40 % and LED power of 80 %, at 22 °C
9 temperature. Same protocol was followed for the W32A mutant as well, to assess the binding
10 efficiency of Lig9. The fluorescence data was normalized to fraction bound (0 = unbound, 1 =
11 bound), and the binding constants (K_d) were determined using the equation derived from the
12 law of mass action.

13 14 ***Fluorimetric study of ligands on tryptophan oxidation***

15 The kinetic profile of protein tryptophan (Trp) residue consumption induced by AAPH-derived
16 radicals was assessed by fluorescence spectroscopy (Fuentes-Lemus et al., 2016; Manjula et
17 al., 2018). A reaction mixture containing protein (5 μ M) with 6 mM AAPH (2, 20-azobis (2-
18 amidinopropane) dihydrochloride) was incubated in phosphate buffer 100 mM, pH 7.4 at 45
19 °C. Trp consumption was evaluated by the progressive decrease of the fluorescence intensity
20 at 360 nm (excitement wavelength 295 nm). The fluorescence intensity was measured for 90
21 min with 2 min of time intervals. Fluorescence measurements were carried out using a Perkin
22 Elmer LS-55 spectrofluorimeter.

23
24

1 **Results and discussion**

2 *Virtual screening*

3 The objective of the virtual screen was to precisely find compounds that can camouflage the
4 exposed SOD1 tryptophan (Trp32) binding site and the nearby region. AutoDock Vina (Vina,
5 2010) was used to obtain hit compounds from the NCI diversity set III containing 1620
6 molecules. The virtual screening results were ranked based on the predicted binding free
7 energies (ΔG_{vina}). The PyMOL program plugged with AutoDock Vina (Seeliger & de Groot,
8 2010) was used to visually check the predicted binding conformations for the selected
9 conformations from the sorted list. Post-docking visual analysis and cutoff ΔG values filtered
10 out compounds with weak or distal binding to the SOD1 Trp32 surface site. The top 20
11 compounds were selected based on their orientation and levels of interaction with Trp32 and
12 its neighbouring residues (Supplementary Table 1). The analysis revealed that the compounds
13 with simpler heterocyclic composition yielded a better probability of stacking orientation over
14 Trp32 residue to form π - π stacking interactions and acceptable energy values. The shortlisted
15 compounds, intriguingly, contain unique heterocyclic scaffolds like naphthalene, acridine,
16 oxadiazole, etc. throughout except for a few like quinolones (Table 1). The docked poses show
17 an overlay of the heterocyclic ring compounds over Trp32. The presence of charged residues
18 Ser98, Lys30, Asn19 and Glu100 around Trp32 at the protein binding site establishes ligand
19 binding through hydrogen bonding and π -cation interactions with the carboxyl and amide
20 moieties from either the amino acid residues or ligand chemical groups. These five compounds
21 exhibited robust docking interactions with SOD1 (Figure 1) and relatively high binding
22 affinities as determined by SPR assay, described below.

23 *Compound Lig6 (NCI 326182)*

24 The core moiety of Lig6 does not contribute to the π - π interaction with Trp32, instead the
25 benzodioxol component does (Fig 1A). The possibility of π - cation interaction of Lig6 core

1 with Lys30 also plays an important role. The Ser98 exerts ionic interactions with the amino
2 groups from the core moiety, benzodioxol. The dimethyl benzene extension does not interact
3 with the surface residues and is more solvent exposed.

4 ***Compound Lig9 (NCI 127133)***

5 The major interaction of the compound 9 (Lig9) with SOD1 involves the establishment of face
6 to face π - π stacking interactions between the phenanthridine moiety of Lig9 and the indole
7 ring in Trp32 of SOD1 (Figure 1(B)). The amino group of the phenanthridine moiety forms a
8 strong hydrogen bond with Ser98 (1.9 Å). Lys30 shows a higher probability of the formation
9 of π - cation interactions with the phenanthridine ring. The biphenyl component of Lig9
10 remains solvent exposed and does not form any significant interactions with the surface of the
11 protein.

12 ***Compound Lig11 (NCI 135168)***

13 The fluorene moiety of Lig11 overlays tryptophan 32 forming significant π - π stacking
14 interactions (Figure 1(C)). The π - cationic interactions are found to be exhibited by Lys30 on
15 the fluorene moiety. The nitro group attached to the core contributes in the establishment of
16 ionic interactions with Ser98. No other hydrophobic interactions were found to exist because
17 of the burial of hydrophobic side chains of the protein β -sheets.

18 ***Compound Lig13 (NCI 295300)***

19 The benzazepine moiety compound Lig13 contributes to the π - π stacking interactions with
20 Trp32 (Figure 1(D)). The nitrogen atom bearing pyrrole part of the indole moiety in Trp32
21 exerts π - cation interactions on the benzyl ring of Lig12. The foresaid interactions orient the
22 compound in a concave overlay on the protein surface. The amino group of the core moiety
23 contributes to weak hydrogen bonding with Ser98. Additionally, significant ionic interactions
24 are also observed between the amino group of benzazepin in Lig13 and Ser98 residue on SOD1
25 surface.

1 ***Compound Lig15 (NCI 117987)***

2 The best pose of compound Lig15 is oriented on the Trp32 residue through π - π stacking
3 interactions (Figure 1(E)). The anthracene ring of the compound plays a pivotal role in the
4 formation of the interactions with the protein surface. The nitrogen atoms on Lys30 and the
5 indole moiety of Trp32 contribute to the formation of π - cation interactions with the anthracene
6 and benzyl moiety of Lig15, respectively. The carboxyl group and one of the oxygen atoms
7 from the dioxo group attached to the anthracene ring contributes to weak electrostatic
8 interactions with Ser98 and Asn96, respectively.

9
10 ***Surface plasmon resonance assay***

11 The 20 compounds short-listed by analysis of docking were procured from National Cancer
12 Institute (NCI) at Bethesda, USA. Five out of 20 compounds exhibited a robust interaction with
13 SOD1 (Figure 2(A)). Compound Lig9 presented the best binding interaction. Analysis of the
14 binding efficiency of Lig9 with SOD1 was performed through surface plasmon resonance
15 (SPR) assays. For SPR analysis, different concentrations of Lig9 were used which yielded
16 concentration-dependent binding as expected (not shown). The binding efficiency was
17 compared between wild SOD1 and W32A mutant of SOD1 (Figure 2(B)). To check the W32
18 interaction with Lig9 both SOD1 and W32A were immobilized to a sensor chip and the on and
19 off rates for ligand binding were recorded on a BIAcore 3000. The recorded sensorgrams show
20 that Lig9 interaction efficiency with the wild-type SOD1 protein is high compared to the W32A
21 mutant (Figure 2(B)).

22
23 ***Crystal structure of the SOD1-Lig9 complex***

24 The five compounds, short-listed from the SPR assay, were used for X-ray studies. High-
25 resolution X-ray diffraction data from crystals soaked with these five compounds were
26 collected and their structures determined by molecular replacement. The SOD1-Lig9 complex,

1 diffracted to 2.5 Å resolution, was crystallized in the C222₁ space group with five SOD1 dimers
2 and one ligand in the asymmetric unit. Chain G of this crystal structure has no visible electron
3 density corresponding to the loop IV (aa: 67-79) and loop VII (aa: 126-141) regions. This may
4 be due to the absence of Zn ion in this chain. Although the Cu ion is missing in the complex,
5 the overall tertiary structure of the complex is very similar to the known typical SOD1
6 homodimer (Parge et al., 1992). The crystallographic and refinement data are summarized in
7 Table 2.

8 The Lig9 molecule binds on the interface formed by chain F (of EF dimer) and chain I
9 (of IJ dimer) (Figure 3(A) and (B)). Electron density for the ligand, Lig9 (NSC127133) was
10 clearly visible in the difference Fourier map (Figure 3(C)). The phenanthridinone moiety and
11 the indole ring of Trp32 (chain F) creates $\pi - \pi$ interactions between them. It successfully
12 camouflages the tryptophan moiety of SOD1. In addition, intermolecular hydrophilic
13 interactions are also observed between O29 atom of Lig9 and the backbone N atom of Ile99
14 (Figure 3(D)). Glu100 residue contributes a $\pi -$ cationic interaction with phenyl-benzoic acid
15 group of Lig9. Water molecules bridge the hydroxy atom of the phenanthridinone moiety and
16 Asp96. The carboxyl oxygen near the phenyl moiety of Lig9 interacts very closely to form a
17 hydrogen bond with Ser988 of SOD1. The phenyl group lays sandwiched between the residues
18 Lys30, Glu100 and Ser98. The crystallographic structure, where we can find significant ligand
19 and protein interactions, correlates well with our SPR analysis. When comparing the docked
20 pose of Lig9 and its crystal structure, the position of the phenanthridinone moiety is very
21 similar. However, the position of carbamoyl linker and phenyl-benzoic acid groups are quite
22 different between the docked and crystal structures (Suppl. Figure S1).

23

24

25

1 ***MD analysis of the wild-type and W32A SOD1 in complex with Lig9***

2 The trajectories generated by molecular dynamic simulations were analyzed for the stability of
3 Lig9 binding near the tryptophan binding site. MD simulations were performed for 50ns. Root
4 mean square deviation (RMSD) analysis (Figure 4(A)) and root mean square per residue
5 fluctuation (RMSF) analysis (Suppl. Figure 2) of the protein backbone dictate the absence of
6 any conformational effects in both the control protein (wild-type SOD1) as well the W32A
7 mutant. But in the presence of Lig9, the RMSD analysis of the ligand position with respect to
8 the protein backbone highlights the loss of binding stability of Lig9 in the W32A complex
9 compared to the wild-type complex (Figure 4B). Notably, a significant loss of intermolecular
10 interactions between the ligand and the W32A-SOD1 protein in the post 20ns simulation time
11 suggesting that W32 is indeed important to make a stable complex with the ligand through $\pi -$
12 π interactions. The RMSF contribution of the individual atoms of the ligand also showed
13 increased fluctuations throughout the simulation time in the mutant dimer compared to the
14 wild-type complex (not shown). Analysis of the radius of gyration (Rg) of the ligand backbone
15 showed the negligible difference between the wild-type and W32A mutant.

16 Visual analysis of the trajectory run revealed the loss of ligand interactions with the
17 binding site when the W32A mutation was incorporated. Towards the end of the simulation,
18 there was a change in the Lig9 binding region as it moved closer to the protein dimer interface.
19 The loss of interaction in the Trp32 site correlates well with the RMSD of the ligand binding
20 with respect to the protein backbone which shows drastic increases in deviation post 20ns
21 simulation time (Figure 4B). A similar fluctuation is also observed in the RMSF graph of the
22 ligand position relative to the protein (not shown). Each ligand atom is found to be fluctuating
23 twice or more with respect to protein position in the mutated W32A SOD1-Lig9 complex.

24 Trajectory cluster analysis provides perspective on the difference in the ligand
25 positioning in wild-type and mutant SOD1. A total of 1042 frames at a step size of 10 from the

1 original set was considered for the cluster analysis. A total of 8 clusters and 24 clusters were
2 obtained in the cluster analysis of the wild-type and W32A complex, respectively (Fig. 5;
3 Suppl. Table 2 and 3). The increase in the number of clusters in the mutated species indicates
4 the instability of the ligand interaction with a particular region, allowing it to explore a wider
5 RMSD matrix from the original reference position. The overlap of the interaction regions in
6 both the cases defines drifting of ligand binding from the W32 binding site in the absence of
7 tryptophan residue, stating its pivotal role in the binding of Lig9 (Figure 5(C)). A close ligand
8 residue analysis throughout the 50ns simulation highlighted the loss of contact with Trp32 by
9 the complete abolishment of $\pi - \pi$ interactions. Taken together, the MD simulations highlight
10 the importance of $\pi - \pi$ interaction is important to obtain a stable complex with SOD1 at the
11 Trp32 binding site. This inference correlates well with both crystallographic and affinity
12 studies.

13 14 ***Microscale thermophoresis (MST) assay***

15 As a quantitative binding assay could not be performed by SPR due to the presence of high
16 DMSO in the Lig9 buffer, MST was carried to evaluate the binding efficiency of Lig9
17 against SOD1 and the W32A mutant. In MST, the binding affinity (K_d) is calculated based
18 on the directional movement of molecules along a temperature gradient, and the protein-
19 ligand interactions are measured using thermophoretic properties of the interacting
20 molecules. The Lig9 compound binding to the native SOD1 results in the binding affinity
21 of $5.7 \pm 1.3 \mu\text{M}$, suggesting that Lig9 significantly binds to SOD1 (Figure 6(A)). As
22 expected, the W32A mutant yielded low binding with a K_d value of $1.2 \pm 0.3 \text{ mM}$ which
23 suggest the importance of the Trp32 for making strong interaction with the ligand.

24

25

26 ***Tryptophan oxidation assay***

1 Next, we assessed the effect of Lig9 binding on the oxidation of SOD1Trp32 using AAPH (2,
2 20-azobis (2-amidinopropane) dihydrochloride), a well-established pro-oxidant that selectively
3 oxidizes Trp residues. The AAPH derived free radicals induce Trp oxidation thereby quenching
4 its fluorescence. The kinetic profile of Trp oxidation was assessed by fluorescence
5 spectroscopy. In the absence of ligands, SOD1 exhibited time-dependent increase in oxidation
6 of Trp residues in the presence of AAPH, as indicated by reduced fluorescence. However, Lig9
7 showed significant inhibition of Trp oxidation (Figure 6(B)). The $\pi - \pi$ stacking interaction of
8 Lig9 with the Trp32 residue of SOD1 is indeed contributed more to the oxidation inhibition, in
9 addition to the electrostatic interaction due to dihydroxy phenyl moiety of Lig9.

10

11 ***Comparison between the Lig9 and SBL1 complexes***

12 We have recently reported the crystal structure of a naphthalene-derived, designed compound
13 (SBL1) in complex with SOD1 (Kershaw et al., 2013; Manjula et al., 2018) (PDB Id: 5YTO).
14 The SBL1 molecule also binds near the Trp32 site. The naphthalene moiety exhibits $\pi - \pi$
15 interactions with the indole ring of Trp32 (site 1), while the dihydroxy phenyl moiety is
16 positioned in a small hydrophilic shallow pocket formed by the loop II connection of β -strands
17 β 2 and β 3 (site 2). Notably, the present Lig9 complex structure suggests a new secondary
18 hydrophilic site (site 2') (described below). Comparison of Lig9 and SBL1 complexes indicates
19 the binding modes of these compounds are similar; however, the interaction exerted by Trp32
20 with the naphthalene and phenanthridine moiety of SBL1 and Lig9 respectively, do not overlap
21 atom for atom (Figure 7(A)). Intriguingly, the positioning of the dihydroxy phenyl moiety and
22 the phenyl benzoic acid moiety of SBL1 and Lig9, respectively, are different; but, both
23 recognize hydrophilic regions. The side chain conformations of the binding site residues,
24 including Trp32, also differ because of the changes in the interactions of both compounds. The
25 side-chain conformations of Lys23 and Lys30 are quite different in each case. The common
26 boundary of the site 2 and site 2' is defined by the orientation of the side-chain of Lys30. Minor

1 rotational variations were found on the carboxylate heads of both Glu21 and Glu100. Glu100
2 is an important residue for hydrophilic interactions with the moiety whether it is in site 2 or
3 site 2'. Overall, our recently reported structure and the present structure revealed an alternative
4 hydrophilic site (site 2') which may need to be considered, besides site 1 and site 2, when
5 developing small molecules by computational studies.

6 7 ***Comparison between the Lig9, aniline and Quinazoline complexes***

8 The crystal structures of aniline in complex with L38V SOD1 (PDB Id: 2WZ0) and a
9 quinazoline derivative with G93A SOD1 (PDB Id: 2WZ6) have been reported (Antonyuk et
10 al., 2010). Superposition of these complexes revealed that the phenanthridinone moiety of
11 Lig9, aniline and quinazoline bind to SOD1 in a similar manner (Figure 7(B) and (C)). The
12 main difference between them in the 'site 1' region is that the indole ring of Trp32 is flipped
13 to form proper $\pi - \pi$ interactions with the respective cyclic ring moiety of these ligands. The
14 side chain conformation of Glu21 is also different in the hydrophilic binding pocket. These
15 conformational changes are required to accommodate the ligand in the Trp32 site and to avoid
16 a steric clash between Trp32 and Glu21.

17 18 **Conclusion**

19 Despite decades of effort there is still no cure for ALS. Drug molecules designed and tested for
20 application in familial ALS should have the capacity to stabilize the SOD1 dimer and prevent
21 aggregation. Our studies infer that, in addition to these properties, ligands that prevent SOD1
22 Trp32 oxidation have therapeutic potential. Virtual screening against the NCI Diversity set III
23 dataset and the SPR binding assay yielded five potential compounds that bind to SOD1. From
24 those five compounds, we have shown that a phenanthridinone derivative (Lig9) binds *in*
25 *crystallo* to SOD1 at the Trp32 site. In addition, a 50ns MD study showed that ligand binding
26 is and suggested the importance of $\pi - \pi$ interactions with Trp32. A binding study using SPR

1 and MST correlate well with the crystal structure of SOD1-ligand complex. Moreover, a Trp-
2 oxidation assay confirmed that the Lig9 molecule significantly inhibits Trp32 oxidation in
3 SOD1. We propose, based on the crystal structures of the Lig9 and SBL1 complexes, that (i)
4 site 1 is pivotal to protect the oxidation of Trp by making $\pi - \pi$ interactions with ligand, and
5 (ii) the hydrophilic sites (site 2 and site 2'), containing critical interacting residues Glu21,
6 Lys30, Ser98 and Glu100, play an important role in making stable SOD1-ligand binding
7 interactions. Chemical modifications of Lig9 in the terminal phenyl-benzoic acid ring portion
8 may help to improve the binding of phenanthridinone derived compounds with SOD1. Thus,
9 the discovered compound, Lig9, can serve as an excellent template, to identify novel
10 phenanthridinone based SOD1 modulators.

11

12

13

14

15

1 **Acknowledgements**

2 BP is grateful to the Department of Biotechnology (DBT), Government of India
3 (BT/PR7079/BID/7/426/2012), SERB-Department of Science and Technology (DST),
4 Government of India (SR/SO/BB-0108/2012), and ICMR, Government of India
5 (BIC/12(19)/2012), for the financial support (SR/SO/BB-0108/2012). MR is thankful to
6 Council of Scientific and Industrial Research (CSIR) for SRF fellowship (09/490(0093)2012-
7 EMR-1). We thank Dr. S. Ramasamy, NCBS for providing the X-ray diffractometer facility.
8 We thank Prof. Samar Hasnain and Dr. Svetlana Antonyuk, University of Liverpool, UK, for
9 providing the human SOD1 clones and for consistent discussions. We thank the Drug Synthesis
10 and Chemistry Branch, Developmental Therapeutics Program, Division of Cancer Treatment
11 and Diagnosis, NCI, USA for providing the compounds used in the study. We also thank Dr.
12 Sivaramaiah Nallapeta & Dr. Saji Menon, NanoTemper Technologies, India, for supporting us
13 with MST analysis by providing Monolith NT.115.

14

15

References

- 1
2
3 Antonyuk, S., Strange, R. W., & Hasnain, S. S. (2010). Structural Discovery of Small
4 Molecule Binding Sites in Cu– Zn Human Superoxide Dismutase Familial
5 Amyotrophic Lateral Sclerosis Mutants Provides Insights for Lead
6 Optimization. *Journal of Medicinal Chemistry*, 53(3), 1402-1406.
- 7 Banci, L., Bertini, I., Boca, M., Girotto, S., Martinelli, M., Valentine, J. S., & Vieru, M.
8 (2008). SOD1 and amyotrophic lateral sclerosis: mutations and oligomerization. *PLoS*
9 *One*, 3(2), e1677.
- 10 Brown, R. H., & Al-Chalabi, A. (2017). Amyotrophic lateral sclerosis. *New England*
11 *Journal of Medicine*, 377(2), 162-172.
- 12 Bruijn, L. I., Houseweart, M. K., Kato, S., Anderson, K. L., Anderson, S. D., Ohama, E.,
13 & Cleveland, D. W. (1998). Aggregation and motor neuron toxicity of an ALS-linked
14 SOD1 mutant independent from wild-type SOD1. *Science*, 281(5384), 1851-1854.
- 15 Chen, V. B., Arendall, W. B., Headd, J. J., Keedy, D. A., Immormino, R. M., Kapral, G. J.,
16 ... & Richardson, D. C. (2010). MolProbity: all-atom structure validation for
17 macromolecular crystallography. *Acta Crystallographica Section D: Biological*
18 *Crystallography*, 66(1), 12-21.
- 19 Chen, Y., & Guillemin, G. (2012). The kynurenine pathway. In Amyotrophic Lateral
20 Sclerosis. InTech.
- 21 Cozzolino, M., Amori, I., Pesaresi, M. G., Ferri, A., Nencini, M., & Carrì, M. T. (2008).
22 Cysteine 111 affects aggregation and cytotoxicity of mutant Cu, Zn-superoxide
23 dismutase associated with familial amyotrophic lateral sclerosis. *Journal of*
24 *Biological Chemistry*, 283(2), 866-874.
- 25 Deng, H. X., Hentati, A., Tainer, J. A., Iqbal, Z., Cayabyab, A., Hung, W. Y., ... & Roos,
26 R. P. (1993). Amyotrophic lateral sclerosis and structural defects in Cu, Zn
27 superoxide dismutase. *Science*, 261(5124), 1047-1051.
- 28 Desmond Molecular Dynamics System, D. E. Shaw Research, New York, NY, 2018.
29 Maestro-Desmond Interoperability Tools, *Schrödinger*, New York, NY, 2018.

- 1 Emsley, P., & Cowtan, K. (2004). Coot: model-building tools for molecular graphics. *Acta*
2 *Crystallographica Section D: Biological Crystallography*, 60(12), 2126-2132.
- 3 Fuentes-Lemus, E., Dorta, E., Escobar, E., Aspee, A., Pino, E., Abasq, M. L., ... & López-
4 Alarcón, C. (2016). Oxidation of free, peptide and protein tryptophan residues
5 mediated by AAPH-derived free radicals: role of alkoxyl and peroxy radicals. *RSC*
6 *Advances*, 6(63), 57948-57955.
- 7 Fujisawa, T., Homma, K., Yamaguchi, N., Kadowaki, H., Tsuburaya, N., Naguro, I., ... &
8 Tsuji, S. (2012). A novel monoclonal antibody reveals a conformational alteration
9 shared by amyotrophic lateral sclerosis-linked SOD1 mutants. *Annals of*
10 *Neurology*, 72(5), 739-749.
- 11 Grad, L. I., Guest, W. C., Yanai, A., Pokrishevsky, E., O'Neill, M. A., Gibbs, E., ... &
12 Cashman, N. R. (2011). Intermolecular transmission of superoxide dismutase 1
13 misfolding in living cells. *Proceedings of the National Academy of Sciences*,
14 201102645.
- 15 Johnston, J. A., Dalton, M. J., Gurney, M. E., & Kopito, R. R. (2000). Formation of high
16 molecular weight complexes of mutant Cu, Zn-superoxide dismutase in a mouse
17 model for familial amyotrophic lateral sclerosis. *Proceedings of the National*
18 *Academy of Sciences*, 97(23), 12571-12576.
- 19 Johnston, J. A., Dalton, M. J., Gurney, M. E., & Kopito, R. R. (2000). Formation of high
20 molecular weight complexes of mutant Cu, Zn-superoxide dismutase in a mouse
21 model for familial amyotrophic lateral sclerosis. *Proceedings of the National*
22 *Academy of Sciences*, 97(23), 12571-12576.
- 23 Kato, S., Shimoda, M., Watanabe, Y., Nakashima, K., Takahashi, K., & Ohama, E. (1996).
24 Familial amyotrophic lateral sclerosis with a two base pair deletion in superoxide
25 dismutase 1 gene: multisystem degeneration with intracytoplasmic hyaline inclusions
26 in astrocytes. *Journal of Neuropathology & Experimental Neurology*, 55(10), 1089-
27 1101.
- 28 Kershaw, N. M., Wright, G. S. A., Sharma, R., Antonyuk, S. V., Strange, R. W., Berry, N.
29 G., ... & Hasnain, S. S. (2013). X-ray crystallography and computational docking for

- 1 the detection and development of protein–ligand interactions. *Current Medicinal*
2 *Chemistry*, 20(4), 569-575.
- 3 Kim, S.H., Kim, S.H., Lee, J.H., Lee, B.H., Yoon, H.J., Shin, D.H., Park, S.S., Jang, S.B.,
4 Park, J.S. and Jee, Y.K., (2015) Superoxide dismutase gene (SOD1, SOD2, and
5 SOD3) polymorphisms and antituberculosis drug-induced hepatitis. *Allergy, Asthma*
6 *& Immunology Research*, 7(1), pp.88-91.
- 7 Lang, L., Zetterström, P., Brännström, T., Marklund, S. L., Danielsson, J., & Oliveberg, M.
8 (2015). SOD1 aggregation in ALS mice shows simplistic test tube
9 behavior. *Proceedings of the National Academy of Sciences*, 112(32), 9878-9883.
- 10 Lebedev, A. A., Young, P., Isupov, M. N., Moroz, O. V., Vagin, A. A., & Murshudov, G.
11 N. (2012). JLigand: a graphical tool for the CCP4 template-restraint library. *Acta*
12 *Crystallographica Section D: Biological Crystallography*, 68(4), 431-440.
- 13 Lindberg, M. J., Tibell, L., & Oliveberg, M. (2002). Common denominator of Cu/Zn
14 superoxide dismutase mutants associated with amyotrophic lateral sclerosis:
15 decreased stability of the apo state. *Proceedings of the National Academy of*
16 *Sciences*, 99(26), 16607-16612.
- 17 Manjula, R., Wright, G. S., Strange, R. W., & Padmanabhan, B. (2018). Assessment of
18 ligand binding at a site relevant to SOD 1 oxidation and aggregation. *FEBS letters*,
19 592(10), 1725-1737.
- 20 Messori, A., Trippoli, S., Becagli, P. and Zaccara, G., 1999. Cost effectiveness of riluzole
21 in amyotrophic lateral sclerosis. *Pharmacoeconomics*, 16(2), pp.153-163.
- 22 Minor, W., & Otwinowski, Z. (1997). HKL2000 (Denzo-SMN) Software Package.
23 Processing of X-ray Diffraction Data Collected in Oscillation Mode Methods in
24 Enzymology, *Macromolecular Crystallography*.
- 25 Murshudov GN, Vagin AA and Dodson EJ (1997) Refinement of macromolecular
26 structures by the maximum-likelihood method. *Acta Crystallographica Section D:*
27 *Biological Crystallography*, 53, 240-255.

- 1 Nishitoh, H., Kadowaki, H., Nagai, A., Maruyama, T., Yokota, T., Fukutomi, H., ... &
2 Ichijo, H. (2008). ALS-linked mutant SOD1 induces ER stress-and ASK1-dependent
3 motor neuron death by targeting Derlin-1. *Genes & Development*, 22(11), 1451-1464.
- 4 Niwa, J. I., Yamada, S. I., Ishigaki, S., Sone, J., Takahashi, M., Katsuno, M., ... & Sobue,
5 G. (2007). Disulfide bond mediates aggregation, toxicity, and ubiquitylation of
6 familial amyotrophic lateral sclerosis-linked mutant SOD1. *Journal of Biological*
7 *Chemistry*, 282(38), 28087-28095.
- 8 Parge, H. E., Hallewell, R. A., & Tainer, J. A. (1992). Atomic structures of wild-type and
9 thermostable mutant recombinant human Cu, Zn superoxide dismutase. *Proceedings*
10 *of the National Academy of Sciences*, 89(13), 6109-6113.
- 11 Pokrishevsky, E., Hong, R. H., Mackenzie, I. R., & Cashman, N. R. (2017). Spinal cord
12 homogenates from SOD1 familial amyotrophic lateral sclerosis induce SOD1
13 aggregation in living cells. *PloS One*, 12(9), e0184384.
- 14 Salminen, H., & Heinonen, M. (2008). Plant phenolics affect oxidation of
15 tryptophan. *Journal of Agricultural and Food Chemistry*, 56(16), 7472-7481.
- 16 Sangwan, S., Zhao, A., Adams, K. L., Jayson, C. K., Sawaya, M. R., Guenther, E. L., ... &
17 Do, T. D. (2017). Atomic structure of a toxic, oligomeric segment of SOD1 linked to
18 amyotrophic lateral sclerosis (ALS). *Proceedings of the National Academy of*
19 *Sciences*, 114(33), 8770-8775.
- 20 Seeliger, D., & de Groot, B. L. (2010). Ligand docking and binding site analysis with
21 PyMOL and Autodock/Vina. *Journal of Computer-Aided Molecular Design*, 24(5),
22 417-422.
- 23 Shaw, B. F., Lelie, H. L., Durazo, A., Nersissian, A. M., Xu, G., Chan, P. K., & Valentine,
24 J. S. (2008). Detergent-insoluble aggregates associated with amyotrophic lateral
25 sclerosis in transgenic mice contain primarily full-length, unmodified superoxide
26 dismutase-1. *Journal of Biological Chemistry*, 283(13), 8340-8350.
- 27 Strange, R. W., Yong, C. W., Smith, W., & Hasnain, S. S. (2007). Molecular dynamics
28 using atomic-resolution structure reveal structural fluctuations that may lead to

- 1 polymerization of human Cu–Zn superoxide dismutase. *Proceedings of the National*
2 *Academy of Sciences*, 104(24), 10040-10044.
- 3 Taylor, D. M., Gibbs, B. F., Kabashi, E., Minotti, S., Durham, H. D., & Agar, J. N. (2007).
4 Tryptophan 32 potentiates aggregation and cytotoxicity of a copper/zinc superoxide
5 dismutase mutant associated with familial amyotrophic lateral sclerosis. *Journal of*
6 *Biological Chemistry*, 282(22), 16329-16335.
- 7 Terwilliger, T. C., Grosse-Kunstleve, R. W., Afonine, P. V., Moriarty, N. W., Zwart, P. H.,
8 Hung, L. W., ... & Adams, P. D. (2008). Iterative model building, structure refinement
9 and density modification with the PHENIX AutoBuild wizard. *Acta*
10 *Crystallographica Section D: Biological Crystallography*, 64(1), 61-69.
- 11 Tiwari, A., & Hayward, L. J. (2003). Familial amyotrophic lateral sclerosis mutants of
12 copper/zinc superoxide dismutase are susceptible to disulfide reduction. *Journal of*
13 *Biological Chemistry*, 278(8), 5984-5992.
- 14 Traynor, K. (2017). FDA approves edaravone for amyotrophic lateral sclerosis.
- 15 Trott, O., & Olson, A. J. (2010). AutoDock Vina: improving the speed and accuracy of
16 docking with a new scoring function, efficient optimization, and
17 multithreading. *Journal of Computational Chemistry*, 31(2), 455-461.
- 18 Vagin, A., & Teplyakov, A. (1997). MOLREP: an automated program for molecular
19 replacement. *Journal of Applied Crystallography*, 30(6), 1022-1025.
- 20 Vina, A. (2010). Improving the speed and accuracy of docking with a new scoring function,
21 efficient optimization, and multithreading Trott, Oleg; Olson, Arthur J. *Journal of*
22 *Computational Chemistry*, 31(2), 455-461.
- 23 Wright, G. S., Antonyuk, S. V., Kershaw, N. M., Strange, R. W., & Hasnain, S. S. (2013).
24 Ligand binding and aggregation of pathogenic SOD1. *Nature Communications*, 4,
25 1758.
- 26 Zhang, H., Andrekopoulos, C., Joseph, J., Chandran, K., Karoui, H., Crow, J. P., &
27 Kalyanaraman, B. (2003). Bicarbonate-dependent peroxidase activity of human Cu,
28 Zn-Superoxide Dismutase induces covalent aggregation of protein intermediacy of

1 tryptophan-derived oxidation products. *Journal of Biological Chemistry*, 278(26),
2 24078-24089.

3 Zhang, H., Joseph, J., Crow, J., & Kalyanaraman, B. (2003). Mass Spectral Evidence For
4 Carbonate Anion Radical-induced Post-translational Modification of Tryptophan
5 Residue to Kynurenine in Human Copper, Zinc Superoxide Dismutase. *Free Radical*
6 *Biology and Medicine*, 35, S22.

7

1 **Figure legends**

2 Figure 1. Binding of the compounds (A) Lig6, (B) Lig9, (C) Lig11, (D) Lig13 and (E) Lig15
3 with the SOD1. The respective ligands and the interacting residues are shown using stick
4 representation. The $\pi - \pi$ or $\pi - \text{ionic}$ interactions are indicated by dots on the respective ring
5 structures. Oxygen and nitrogen atoms are colored in red and blue, respectively.

6
7 Figure 2. Surface plasmon resonance (SPR) assay of SOD1-ligand interactions. (A) SPR
8 sensorgram for the binding of screened molecules on SOD1 immobilized on a CM5 chip was
9 obtained at 250 μM ligand concentration. SPR sensorgrams were established at association and
10 dissociation time intervals of 60 sec and 180 sec, respectively. Lig9 showed maximum
11 response compared to other ligands. (B) Sensorgram for the binding of Lig9 on wild and W32A
12 mutant of SOD1 immobilized on a CM5 chip detecting 125 μM and 250 μM of Lig9 with
13 association and dissociation time intervals of 120 and 180 s, respectively. The dose dependency
14 of Lig9 binding indicates the binding efficiency of the compound is higher for wild-type
15 compared to W32A mutant protein.

16
17 Figure 3. The tertiary structure of the SOD1–Lig9 complex. (A) Lig9 binds between chain F
18 of the EF dimer and chain I of the IJ dimer (arbitrary view). (B) Rotation 90° of (A) about its
19 horizontal axis. (C, D) A close-up view of SOD1–Lig9 interaction. $2|\text{Fo}| - |\text{Fc}|$ map contoured
20 at 1.0s in the binding site region of Lig9. The benzoate moiety of Lig9 is not shown as the
21 corresponding electron density is absent. The ligand and interacting residues are shown by
22 sticks. Hydrogen bonds are indicated by a dotted line. $\pi - \pi$ interactions are shown by dots on
23 the ring structures. Water molecules are shown as spheres. The Zn ion is shown by grey
24 spheres.

25

1 Figure 4. Molecular dynamics simulations of the wild-type SOD1 dimer, mutant W32A-SOD1,
2 and their complex with Lig9. (A) The root-mean square deviation (RMSD) of the wild-type
3 SOD1 dimer (black), and the mutant W32A-SOD1 dimer (grey), (B) RMSD of Lig9 in
4 complex with wild-type SOD1 (black), and mutant W32A-SOD1 (grey).

5
6 Figure 5. molecular dynamics simulations of Lig9 in complex with the wild-type SOD1 dimer,
7 and the W32A-SOD1 dimer. (A) Trajectory cluster analysis of the wild-type complex (green
8 mesh), (B) Trajectory cluster analysis of the W32A mutant complex (red mesh), and (C)
9 Overlap view of the clusters shown in (A) and (B). Respective ligands clusters are shown as
10 sticks.

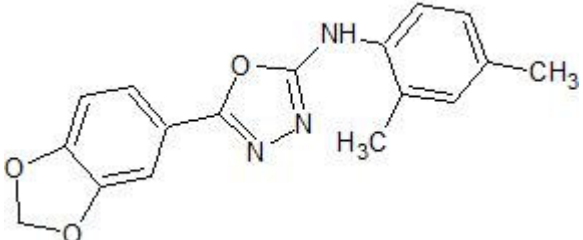
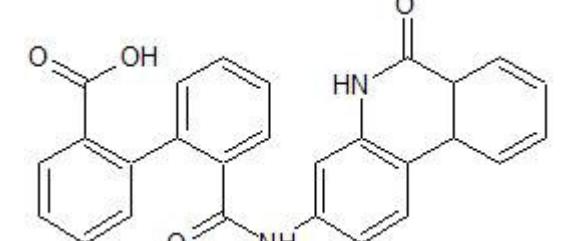
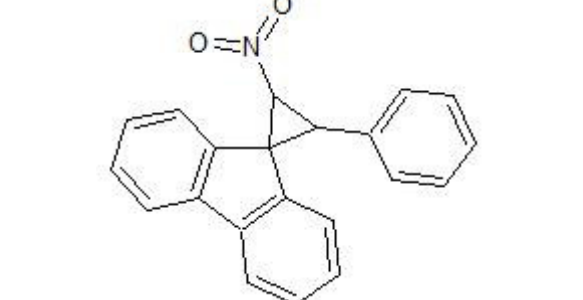
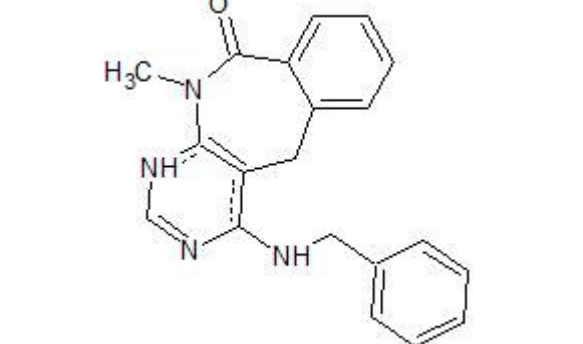
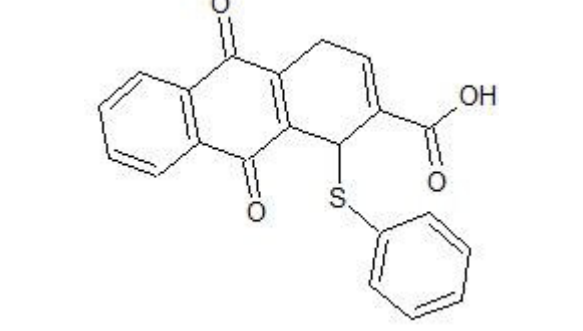
11
12 Figure 6. Microscale thermophoresis (MST) and Trp-oxidation assay. (A) MST interaction
13 analysis of the wild-type and W32A SOD1 proteins with Lig9. Dose-response curves for the
14 binding interaction between Lig9 and native or W32A SOD1. Plots show the fraction bound
15 against the ligand concentration (0 = unbound, 1 = bound). Lig9 shows substantial binding with
16 the wild-type SOD1 (brown) (K_d of $5.7 \pm 1.3 \mu\text{M}$), whereas binding is very weak against the
17 W32A mutant (green) (K_d : $1.2 \pm 0.3 \text{ mM}$) demonstrating the importance of Trp32 for ligand
18 binding. (B) Kinetic profiles of SOD1 Trp32 consumption mediated by AAPH free radicals in
19 the presence and absence of Lig9. The mutant protein W32A was used as a control to check
20 significant deviations in fluorescence emission at 360nm (excitation at 295nm) with time. The
21 kinetic profile of SOD1 in presence of Lig9 was almost the same as the normalized data of
22 W32A.

23
24 Figure 7. Comparison of the SOD1-Lig9 complex and SBL-1. Superposition of the SOD1–
25 Lig9 complex (A) on to the SOD1 – SBL-1 complex (PDB Id: 5YTO). The naphthalene moiety
26 of SBL-1 makes $\pi - \pi$ interactions with SOD1 Trp32 (Site 1). The dihydroxy moiety of SBL-

1 1 binds in the hydrophilic region of Site 2, whereas the benzene group of Lig9 binds in the Site
2 2' hydrophilic region, (B) on to the SOD1-Aniline complex (PDB Id: 2W20). The aniline group
3 contributes $\pi - \pi$ interactions with Trp32 of SOD1, and (C) on to the quinazoline complex
4 (PDB Id: 2WZ6). The quinazoline group contributes $\pi - \pi$ interactions with Trp32 of SOD1.
5 The ligands and interacting residues are shown by sticks. The nitrogen and oxygen atoms are
6 colored in blue and red, respectively. Dotted circles represent Site 1, Site 2, and Site 2'. The
7 Lig9, SBL-1, aniline and quinazoline molecules are colored in olive green, brown, yellow and
8 pink, respectively.
9

1

2 **Table 1: A short-listed compounds based on SPR assay**

Ligand ID	NCI Compound	2D Structure
Lig6	NCI 326182	
Lig9	NCI 127133	
Lig11	NCI 135168	
Lig13	NCI 295300	
Lig15	NCI 117987	

3

1 **Table 2: Crystallographic data collection and refinement statistics.**
2

Data collection parameters	SOD1–Lig9 Complex
Space group	C222 ₁
Cell dimensions a b c (Å)	164.36, 203.69, 144.21
Wavelength (Å)	1.5814
Resolution (Å) [#]	38.43 - 2.5
Unique reflections	83750
R _{merge} [†]	0.079 (0.548)
⟨I/σ⟩	19.7 (2.0)
Completeness (%)	100 (100)
Redundancy	6.5 (5.7)
CC _{1/2} ^{##}	0.824
Wilson plot B-factor (Å ²)	39.1
Refinement	
Resolution (Å)	20.0 – 2.50
No. of reflections	79255
[†] R _{work} / [†] R _{free} (%)	16.6 / 23.7
Total no. of atoms	12350
Protein atoms	11005
Water molecules	1234
DMSO	2
Glycerol molecules	4
Ligand molecules	1
Polysulfane molecules	3
Zn-ion	9
Average B-factor (Å ²)	42.05
RMSD Bonds (Å)	0.032
RMSD Angles (°)	2.77

3

4 [#]Numbers in parentheses are values in the highest resolution shell.5 [†]R_{merge} = $\sum_{hkl} \sum_i |I_i(hkl) - \langle I(hkl) \rangle| / \sum_{hkl} \sum_i I_i(hkl)$, where $I_i(hkl)$ is the intensity of the
6 i^{th} measurement and $\langle I(hkl) \rangle$ is the mean intensity for that reflection.7 [†]R_{work} = $\sum_{hkl} ||F_{obs}| - |F_{calc}|| / \sum_{hkl} |F_{obs}|$, where $|F_{obs}|$ and $|F_{calc}|$ are the observed and
8 calculated structure-factor amplitudes, respectively.9 [†]R_{free} was calculated with 5.0% of reflections in the test set.10 ^{##}Values correspond to the highest resolution shell

11

1 **Supplementary Information:**2 **Supplementary Table 1: Docking scores for the 20 compounds from the NCI diversity set**
3 **III.**

4

Ligand ID	NCI Compound	Dock Score (kcal/mol)	Ligand efficiency (kcal/heavy atom)
Lig1	NCI 84100	-7.5	-0.25
Lig2	NCI 116702	-7.4	-0.2643
Lig3	NCI 55862	-6.9	-0.3
Lig4	NCI 43998	-6.8	-0.2833
Lig5	NCI 60785	-6.7	-0.2481
Lig6	NCI 326182	-6.6	-0.287
Lig7	NCI 156516	-6.5	-0.2167
Lig8	NCI 214009	-6.5	-0.2407
Lig9	NCI 127133	-6.4	-0.1939
Lig10	NCI 13051	-6.3	-0.2172
Lig11	NCI 135168	-6.3	-0.2625
Lig12	NCI 283845	-6.1	-0.2905
Lig13	NCI 295300	-6	-0.24
Lig14	NCI 295486	-6	-0.2308
Lig15	NCI 117987	-5.9	-0.2269
Lig16	NCI 121868	-5.9	-0.1844
Lig17	NCI 170955	-5.9	-0.2682
Lig18	NCI 211490	-5.8	-0.1657
Lig19	NCI 116709	-5.5	-0.2037
Lig20	NCI 163443	-5.1	-0.17

5

1 Supplementary Table 2: Trajectory cluster analysis – SOD1-#10 complex*Cluster no.* No. of members

1	412
2	217
3	152
4	91
5	79
6	50
7	28
8	13

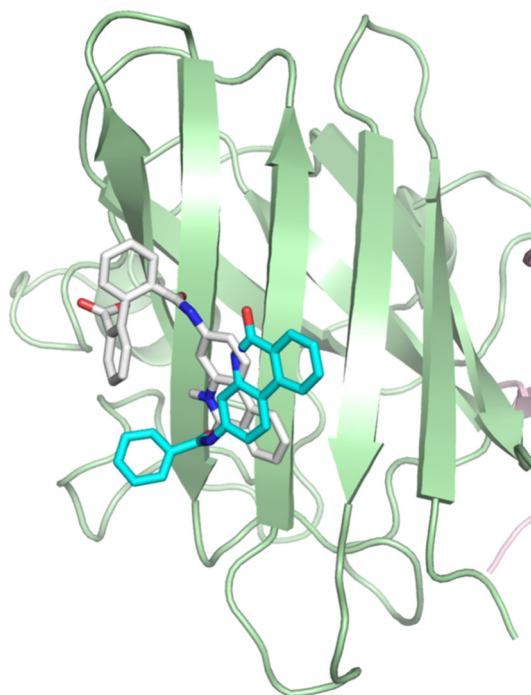
2

3

4 Supplementary Table 3: Trajectory cluster analysis – W32A-#10 complex

<i>Cluster no.</i>	No. of members
1	109
2	93
3	86
4	74
5	55
6	47
7	46
8	44
9	42
10	41
11	40
12	40
13	38
14	35
15	35
16	35
17	33
18	31
19	22
20	21
21	20
22	19
23	19
24	17

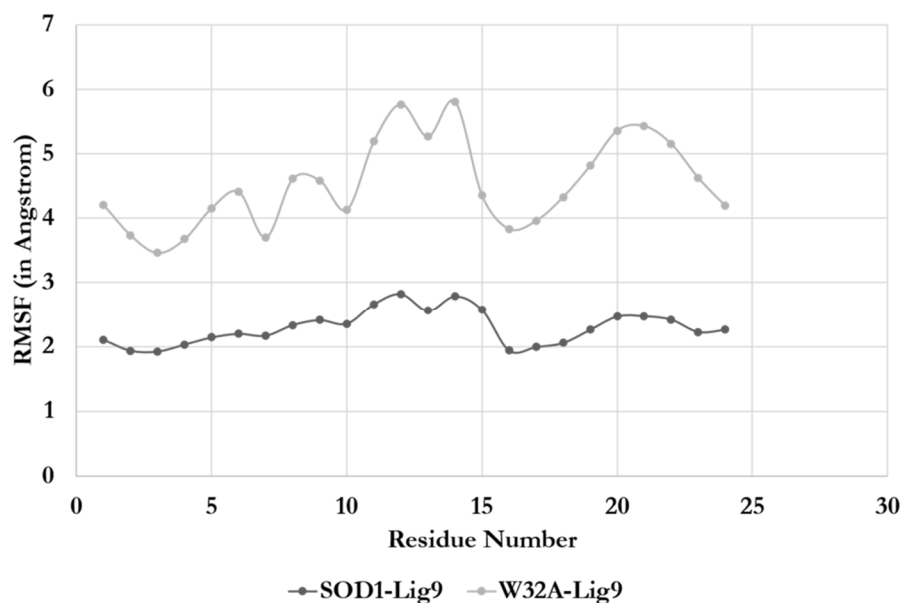
1
2
3
4
5
6
7
8
9
10
11
12
13
14
15
16
17
18
19
20
21
22
23
24
25
26
27
28
29
30



Supplementary Figure S1

Superposition of the crystal structure of the SOD1 – Lig9 complex on to the docked structure. The $\pi - \pi$ interactions with Trp32 of SOD1 are conserved both in the crystal and docked structures.

1
2
3
4
5
6
7
8
9
10
11
12
13
14
15
16
17
18
19
20
21
22
23



Supplementary Figure S2

The molecular dynamics simulations of the wild-type SOD1 dimer, mutant W32A-SOD1, and their complex with Lig9. The root-mean square fluctuations (RMSF) of the wild-type SOD1 dimer (black), and the mutant W32A-SOD1 dimer (grey).